Nuclear Materials and Energy 33 (2022) 101265

Contents lists available at ScienceDirect

Nuclear Materials and Energy

journal homepage: www.elsevier.com/locate/nme

Spectroscopic investigation of the tungsten deuteride sputtering in the EAST divertor

Q. Zhang [a,b], F. Ding [a,*], S. Brezinsek [c], L. Yu [a,b], L.Y. Meng [a], P.A. Zhao [a,b], D.W. Ye [a,b], Z.H. Hu [a], Y. Zhang [a], R. Ding [a], L. Wang [a], G.-N. Luo [a,b], EAST Team

[a] Institute of Plasma Physics, HFIPS, Chinese Academy of Sciences, Hefei 230031, China
[b] University of Science and Technology of China, Hefei 230026, China
[c] Forschungszentrum Jülich GmbH, Institut für Energie-und Klimaforschung-Plasmaphysik, Partner of the Trilateral Euregio Cluster (TEC), 52425 Jülich, Germany

ARTICLE INFO

Keywords:
Tungsten
Plasma-facing materials
Sputtering
EAST
Divertor

ABSTRACT

Physical sputtering caused by particle bombardment is believed to be the main erosion mechanism of W materials in fusion devices, in which W atoms are the sputtering products. However, the tungsten deuteride molecule (WD) spectra have been observed in both TEXTOR and ASDEX Upgrade, which was believed to be the product of chemically assisted physical sputtering (CAPS), a new sputtering mechanism that has been proposed in recent years. In this paper, we report the spectroscopic observation of WD molecules in the EAST W divertor. The behaviors of WD molecules sputtering are compared with W atoms sputtering via the spectral measurements of the ro-vibrational band emission of WD $^6\Pi \rightarrow {}^6\Sigma^+$ in the spectral range between 673 nm and 678 nm and the WI line emission at 400.9 nm. The physical sputtering characters and chemical sputtering characters of WD molecule sputtering were confirmed in EAST. The measurements in EAST showed that there is an energy threshold for WD molecules sputtering and that the sputtering energy threshold of WD molecules is smaller than that of W atoms. Furthermore, the dependence of WD molecule sputtering efficiency (the absolute WD photon flux (Ph_{WD}) normalized to the particle flux (Γ_{ion}) reaching the target with a constant T_e) on impact energy and heat flux were studied, presenting significantly different behaviors compared with W atom sputtering. In addition, it is found that the decrease of WD sputtering efficiency with the heat flux is accompanied by the rise of the photon flux of D_δ (410.06 nm) normalized to the particle flux (Γ_{ion}) at the divertor target, which may imply the enhanced deuterium desorption at the W surface. The further increase of heat flux hitting the target surface could elevate the surface temperature and benefit the deuterium release from the surface, which may influence the formation of WD molecules at the surface layer.

1. Introduction

Tungsten (W) is selected as a plasma-facing material (PFM) for the ITER divertor due to its high melting temperature, high thermal conductivity, and low fuel retention [1–5]. However, the lifetime of the W divertor is limited by the erosion processes during plasma discharge periods. Moreover, W is a strong radiator in the core plasma, thus the central concentration of W impurity must be kept at or below 10^{-5} to avoid the radiative cooling by W ions [6,7]. Therefore, W erosion is one of the issues in fusion reactors. EAST has been equipped with W upper divertor since 2014, and W lower divertor since 2021, which helps understand the W erosion in the divertor region [8,9].

Previous research on W erosion has focused on Physical Sputtering (PS) processes caused by impinging particles [10,11]. While in 2019, S. Brezinsek and his colleagues discovered for the first time, in addition to the bare PS processes, a second W erosion mechanism in TEXTOR (limiter surfaces) and ASDEX Upgrade (divertor target plates) during deuterium plasma bombardment [4]. This mechanism has been identified as Chemically Assisted Physical Sputtering (CAPS), which leads to the formation of the tungsten deuteride molecule WD identified spectroscopically via the $^6\Pi \rightarrow {}^6\Sigma^+$ transition. Measurements in TEXTOR and ASDEX Upgrade showed a dependence of the WD band emission on the surface temperature - connected to the deuterium content in the near W surface - as well as on the flux and energy of impinging energetic particles [4]. In 2020, L. Ballauf and his colleagues observed the W^+ and W_2^+ of physical sputtering (PS) and WD^+ of CAPS in ion beam-type

* Corresponding author.
E-mail address: fding@ipp.ac.cn (F. Ding).

https://doi.org/10.1016/j.nme.2022.101265
Received 29 June 2022; Received in revised form 27 September 2022; Accepted 29 September 2022
Available online 30 September 2022

experiments, and concluded that bare W^+ and W_2^+ were seen to be sputtered more at elevated ion impact energies and increasing surface temperatures, while the relative yield of WD^+ was enhanced at higher impact energies, but diminished with increasing tungsten temperature [12]. The sputtering behavior of WD molecules is quite different from that of W atoms.

To better understand W erosion in fusion devices, here we provide further insight into the WD sputtering and W sputtering processes in EAST. The multichannel visible spectroscopy system (MVSS) allows observation and analysis of the WD band emission of the WD transition $^6\Pi \rightarrow {}^6\Sigma^+$ between $\lambda = 673$ nm and $\lambda = 678$ nm and the neutral W line emission of the WI transition $(5d^5(^6S)6s^7S_3 \rightarrow 5d^5(^6S)6p^7P_4)$ at $\lambda =$ 400.9 nm [13]. By analyzing the intensity and position distribution of the WD spectrum, some characteristics of WD sputtering under EAST experimental conditions were obtained and a comparison between WD molecules and W atoms sputtering was carried out.

Section 2 has introduced the spectroscopy system (MVSS) monitoring the W divertor region in EAST. Section 3 focuses on the similarities and differences between the sputtering behaviors of WD molecules and W atoms. In this section, the existence of the energy threshold for WD sputtering is discussed and a comparison between the energy threshold of WD sputtering and that of W sputtering is carried out. Moreover, the dependences of WD and W sputtering on incident energy as well as the heat flux hitting the W target surface are also investigated. The possible reasons are suggested based on the experimental observations. In the last section, a summary is presented.

2. The experimental setup and relevant diagnostics

A dedicated multichannel visible spectroscopic diagnostic system has been developed for monitoring impurity behavior by collecting impurity spectra information in the divertor area in EAST [13]. There are 22 lines-of-sight (LOSs) viewing the upper outer (UO) divertor, achieving a 13 mm spatial resolution along the target surface, and 22 LOSs viewing the lower outer (LO) divertor, achieving a spatial resolution <25 mm, as shown in Fig. 1. The time resolution herein was normally set as about 5 ms so that 22 LOSs can be acquired simultaneously by the Electron-Multiplying Charge Coupled Device (EMCCD) detector [14]. The multichannel emission lights are transferred via optical fibers and detected simultaneously by the spectrometer with EMCCD. In addition, the ion flux density j_s ($\Gamma_{ion} = j_s/e$), divertor electron temperature T_{et} and vertical heat flux q_t are measured by Langmuir probes (LP) on the upper and lower divertor targets [15].

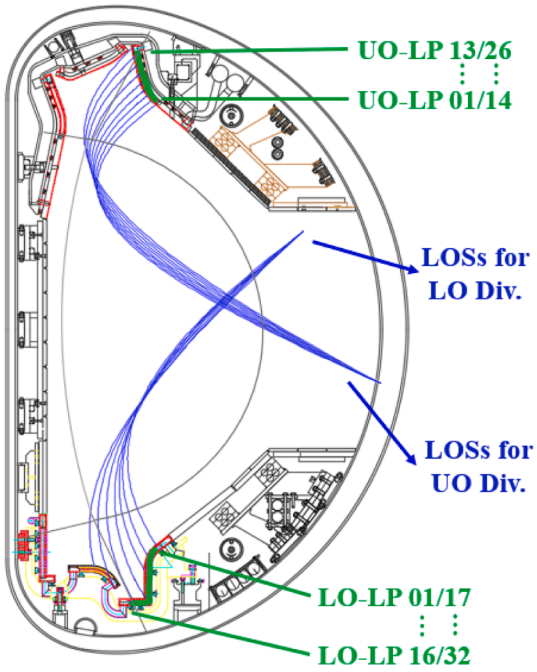

Fig. 1. A poloidal cross-section of EAST with the main diagnostics used in this work. The blue lines are the spectroscopic lines-of-sight (LOSs) viewing the UO and the LO divertors, and the green points are the Langmuir probes on the UO and LO divertors. (For interpretation of the references to colour in this figure legend, the reader is referred to the web version of this article.)

Fig. 2(a) shows the WD molecular band spectrum observed in TEXTOR [4], and Fig. 2(b) shows a typica band spectrum obtained from the UO divertor region in EAST, confirming the existence of WD molecular sputtering in EAST. The main spectroscopic features of the WD band spectrum – the line-like shape of the Q-branch at $\lambda = 674.48$ nm, the returning R-branch at the lower wavelength end at $\lambda = 673$ nm and the long P-branch tail in the higher range up to $\lambda = 678$ nm – are clear. The line-like Q-branch was used as the characteristic peaks of the WD molecular band spectrum to analyze the spectral intensity and sputtering position distribution.

Both WD Q-branch and W I 400.9 nm radiances were estimated as integrated intensity for the defined wavelength regions (674.18–674.78 nm for WD Q-branch and 400.6–401.2 nm for W I 400.9 nm). The sputtered W atom flux at divertor target can be inferred from the absolute W I photon flux by using the so-called *S/XB* coefficient, i.e. inverse photon efficiency method [16], which is commonly applied in the *in situ* W erosion studies [17]. However, For WD molecular sputtering, similar methods cannot be used because the so-called *D/XB*-values, which provides the ratio of ionization and dissociation rate coefficients (the *D* for decay) of the WD molecule over the excitation rate coefficient *X* for the observed $^6\Pi \rightarrow {}^6\Sigma^+$ multiplied with the Branching ratio *B*, are currently unknown [4]. According to experiments and literature, The *D/XB* values are closely related to divertor electron temperature T_{et} [4,18,19]. We assume that within a small range of variation in T_{et}, the *D/XB* values for WD are comparable so that the photon flux normalized to the particle flux reaching the target (Γ_{ion}) - Ph_{WD}/Γ_{ion} - can be used to discuss the quantitative changes in WD molecules sputtering. And for W atoms sputtering, the obtained *S/XB* values for W show that when $T_{et} >$ 10 eV, Ph_{WI}/Γ_{ion} can also reflect the quantitative changes in W atoms sputtering within a small range of variation in T_{et} [16]. Therefore, in this article, the changes in WD molecules sputtering and W atoms sputtering are quantitatively discussed by using the values of Ph_{WD}/Γ_{ion} and Ph_{WI}/Γ_{ion} under the premise that the variation range of T_{et} is small. Meanwhile, the spatial distribution of spectrum signals along the target is employed to derive the difference in sputtering characteristics between WD molecules and W atoms.

3. Experimental results and discussions

3.1. Incident energy dependence and energy threshold for WD molecular sputtering

Threshold energy (E_{th}) of impact exists for Physical Sputtering of W. For example, the E_{th} of D, He, and C to sputter W from the divertor target are 220, 110 and 80 eV, respectively [20]. Experiments in non-fusion devices - ion beam-type experiments for ablation of tungsten surfaces in collisions with Ar^+, He^+ and N_2^+ cation projectiles in the presence of D_2 - indicate a minimum energy requirement for the chemically assisted sputtering of WD^+ [12]. And for fusion devices, the release mechanism of WD molecules is thought to happen via cascades followed by a release so that the minimum impact energy is also required [4], That is to say, an energy threshold for WD sputtering should also exist. However, more details on the existence of energy threshold for WD molecular sputtering have not been studied.

Fig. 3 shows the key plasma parameters of an L-mode discharge (#87702) in EAST, including the time evolution of the line-averaged density ($_{el}$) in core plasma (Fig. 3(a)) as well as the electron density (n_{et}) (Fig. 3(b)), the ion flux density (j_{st}) (Fig. 3(c)),and the electron

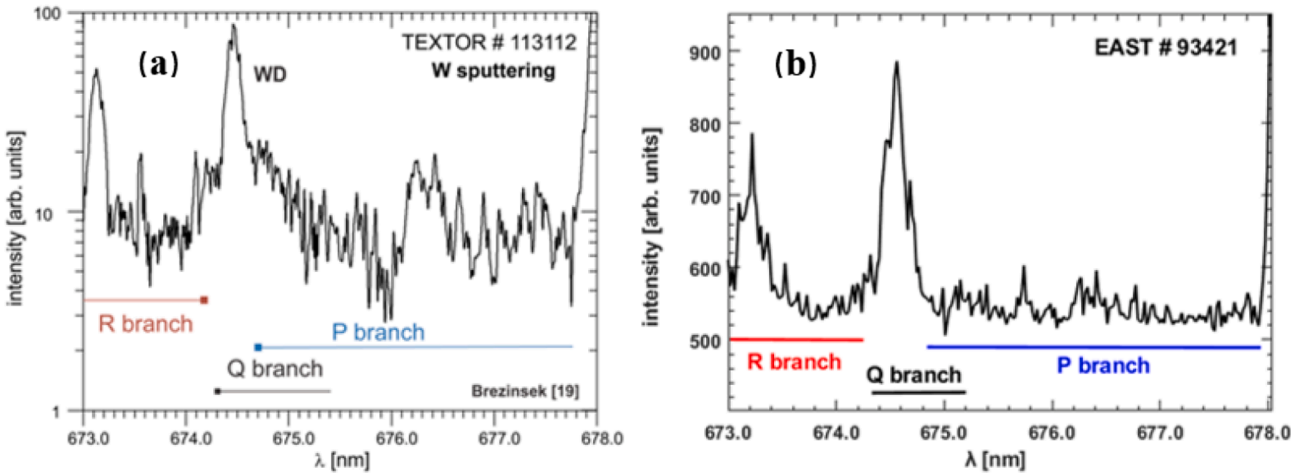

Fig. 2. (a) The WD molecular band spectrum observed in TEXTOR [4], and (b) the band spectrum in EAST.

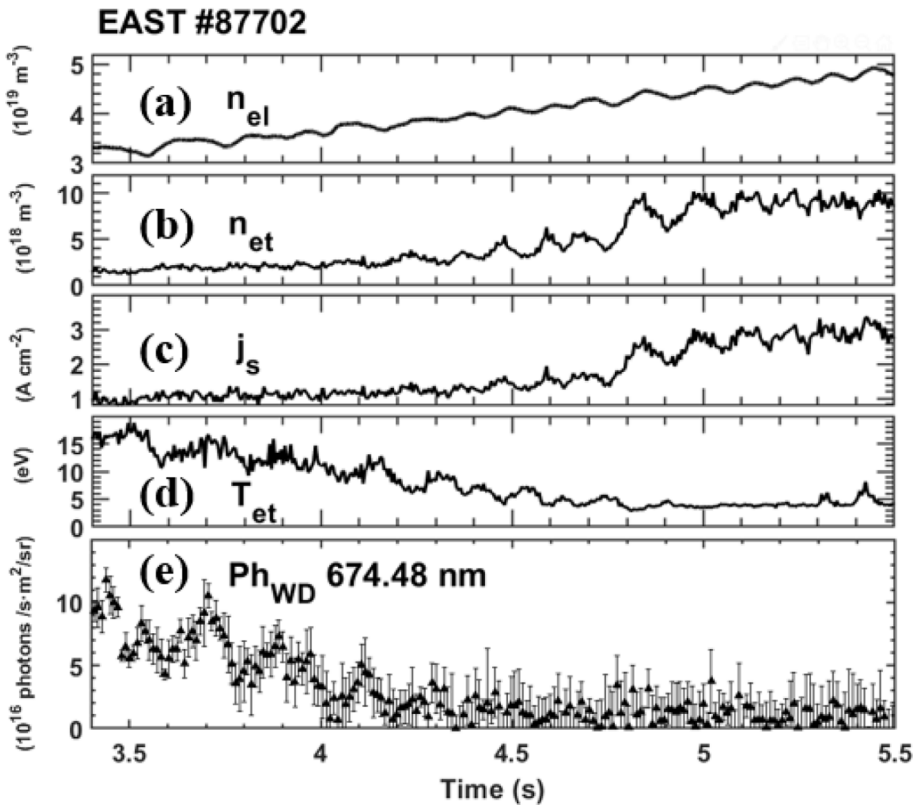

Fig. 3. Time evolutions of the key plasma parameter for #87702. The panels from top to bottom represent (a) the plasma line-averaged density ($_{el}$), (b) the electron density at the UO target (UO n_e), (c) the ion flux density at the UO target (UO j_s), (d) the electron temperature at the UO target (UO T_e) and (e) the absolute WD photon flux (Ph_{WD}).

temperature (T_{et}) (Fig. 3(d)) in the upper outer (UO) divertor. As the $_{el}$ ramps up from 3×10^{19} m^{-3} to 5×10^{19} m^{-3}, the n_{et} and j_{st} increase while the T_{et} decreases. Fig. 3(e) shows the variation of the radiance of the line-like Q-branch of the WD $^6\Pi \rightarrow {}^6\Sigma^+$ band emission and indicates that as j_{st} and n_{et} increase and T_e decreases, the WD radiance drops significantly, especially when T_e is reduced to only a few eV, the WD radiance disappears (After 4.3 s, the WD radiance fluctuates at the background level, and the spectral signal measured by the spectrometer has no shape of the WD band).

In order to more clearly analyze the WD radiance at low T_{et}, WD radiance as a function of T_{et} is plotted in Fig. 4. While T_{et} is a measure for the impact energy via $E_{in} = 3k_BT_e + 2k_BT_i$ and $T_e \approx T_i$ with the ion temperature T_i [20]. Fig. 4 shows two phenomena, one of which is that the WD radiance decreases as T_{et} decreases until around 8 eV, and the other is that WD radiance disappears when $T_{et} < 8$ eV, although the incident particle flux is still increasing. The first phenomenon is similar to the previous observations in TEXTOR which verified the physical sputtering character of CAPS – reduction of WD with reduction of T_{et}, or more precisely impact energy E_{in}. The second phenomenon indicates that an energy threshold is existed for the WD sputtering in EAST, because the decrease of T_{et} indicates the decrease of impact energy E_{in}. When $T_{et} < 8$ eV, the energy carried by the incident particles will not be sufficient to sputter out WD molecules.

Fig. 5 shows the WD bands measured by the spectrometer at $T_{et} =$

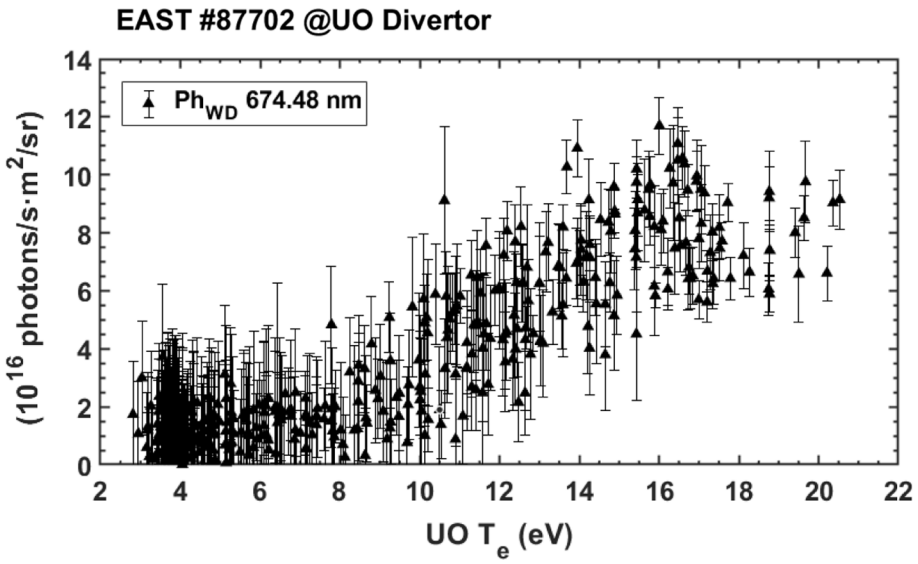

Fig. 4. WD radiance as a function of T_{et} for 87,702 at UO divertor.

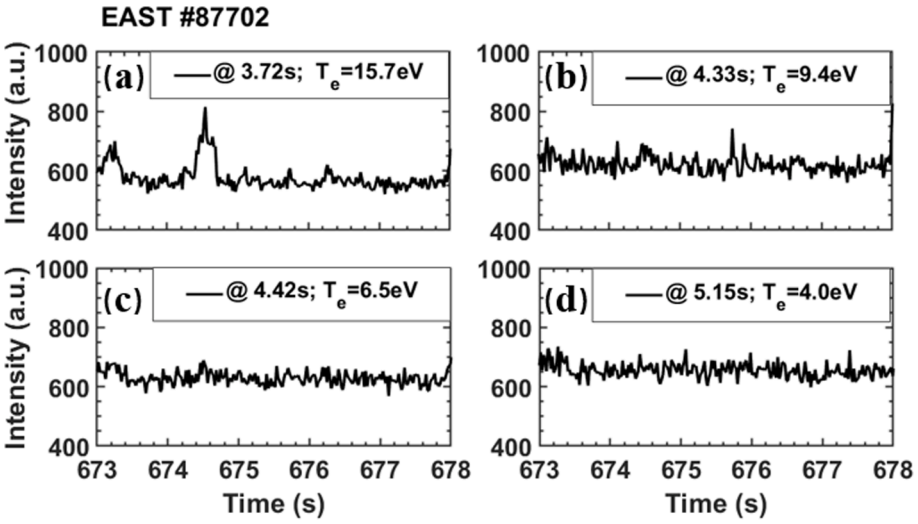

Fig. 5. The WD molecular band observed at the UO divertor in several seconds for 87702.

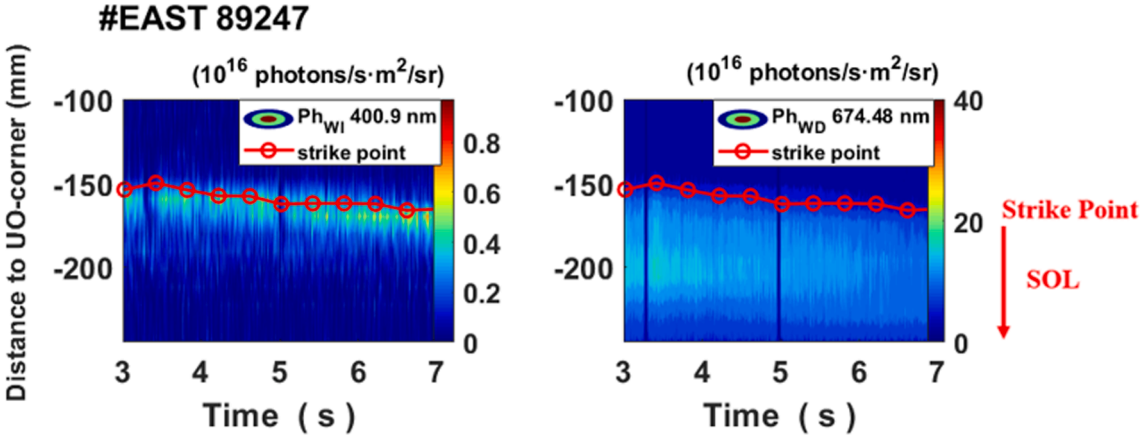

Fig. 6. The poloidal distribution of the photon flux of W I and WD at the UO divertor.

15.7 eV, $T_{et} = 9.4$ eV, $T_{et} = 6.5$ eV, and $T_{et} = 4$ eV, respectively. When $T_{et} < 8$ eV, the shape of the WD band does not exist, confirming that there is no WD molecular sputtering. The energy threshold requirement for WD sputtering may be related to its release mechanism – by cascading collisions [4]. Cascade collisions require enough energy to bombard the particles outside the target. It should be noted that, the T_{et} of 8 eV reflecting the energy threshold is obtained in this shot, and may be subject to the influences of other elements, such as surface deposition layer, impurity concentration etc.

Spectroscopic observations in EAST also show that the distribution range of W atom sputtering and WD molecule sputtering at the UO divertor is different. Fig. 6 shows the poloidal distribution of the photon flux of WI transition ($5d^5(6S)6s^7S_3 \rightarrow 5d^5(6S)6p^7P_4$) and WD transition ($^6\Pi \rightarrow {}^6\Sigma^+$) at the UO divertor during an L-mode discharge #89247, in which the red lines mark the locations of the strike point. The sputtering range of the W atom is narrower and concentrated near the strike point while the sputtered WD molecules are distributed in a wider area, extending to the far Scrape-Off Layer (SOL) region. This may be due to the different sputtering energy thresholds of W atom and WD molecular, because in the SOL region farther from the strike point, the incident particle energy is lower than that near the strike point.

The discharge parameters in discharge #89247 are shown in Fig. 7 with a plasma current of $I_p = 0.45$ MA, a plasma line-averaged density of $_{el} = 1.4 \times 10^{19}$ m^{-3} and a total input power of $P_{in} = 1.4$ MW. As can be seen from Fig. 7(a)–(e), the parameters are stable during 3–7 s. Meanwhile, the strike point keeps at 162 mm to the corner of the UO divertor during 3–7 s. Therefore, 5 different positions from strike point to farther SOL region (as shown in Fig. 7(f)) are chosen to calculate the average values of WI and WD radiance at each position during 3–7 s. The results are shown in Fig. 8.

Fig. 8 plots the W I and WD radiances at five different positions on the UO target. It can be seen that far from the strike point, W I radiance drops rapidly and disappears at the position of 233 mm away from the corner of the UO divertor ($T_{et} = 9.7$ eV), while the WD radiance is still strong at this position. This indicates that the sputtering energy thresholds of W atoms and WD molecules may be different. The sputtering energy threshold of WD is lower than that of W atoms. Therefore, at locations with lower impact energy, WD molecules still be sputtered, despite the disappeared W atom sputtering. Notably, the peak positions of WD and W I radiance are also different. This may be related to the distribution of heat flux incident on the divertor, which will be discussed in the next section.

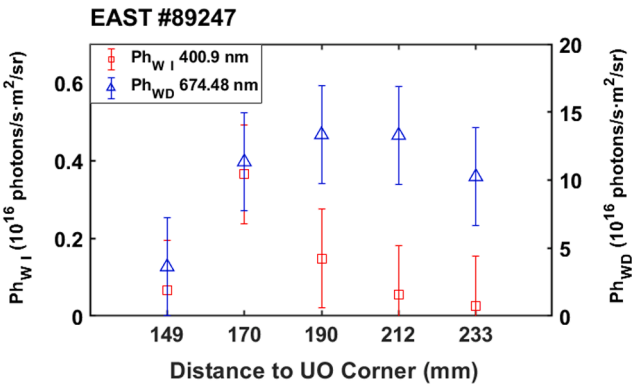

Fig. 8. The average values of WD and WI radiance at different poloidal positions during 3–7 s of discharge #89247.

The reason for the lower energy threshold for WD sputtering is currently unclear. For the carbon (C) in the first wall of tokamak, deuterium accumulation on the wall surface will reduce the surface binding energy according to the research of S.G. Liu et al. [21,22]. And in the research on the irradiation of H^+ on W materials, B. Yang et al. found that H^+ will reduce the binding energy on the surface of the W film [23]. According to these researches, D^+ bombardment and aggregation may also reduce the surface binding energy of W materials, making the bonds linking W atoms easier to break. Gathering with a large number of D^+, the W atoms are more likely to be sputtered out of the target in the form of WD molecules. This may be the reason why there is still WD sputtering at lower impact energies, however, more detailed experiments and analysis are required to verify this conjecture.

3.2. Influences of heat flux and D retention

As is discussed in Section 3.1, the sputtering distribution of WD molecules clearly differs from that of W atoms along the UO divertor target. Due to the varied T_{et} along the target, it is difficult to accurately compare the variation of sputtering particles of WD molecules and W atoms. According to the *S/XB* theory [4,14,24–26], when T_{et} remains unchanged, the change in Ph_{WD}/Γ_{ion} and Ph_{WI}/Γ_{ion} can reflect the

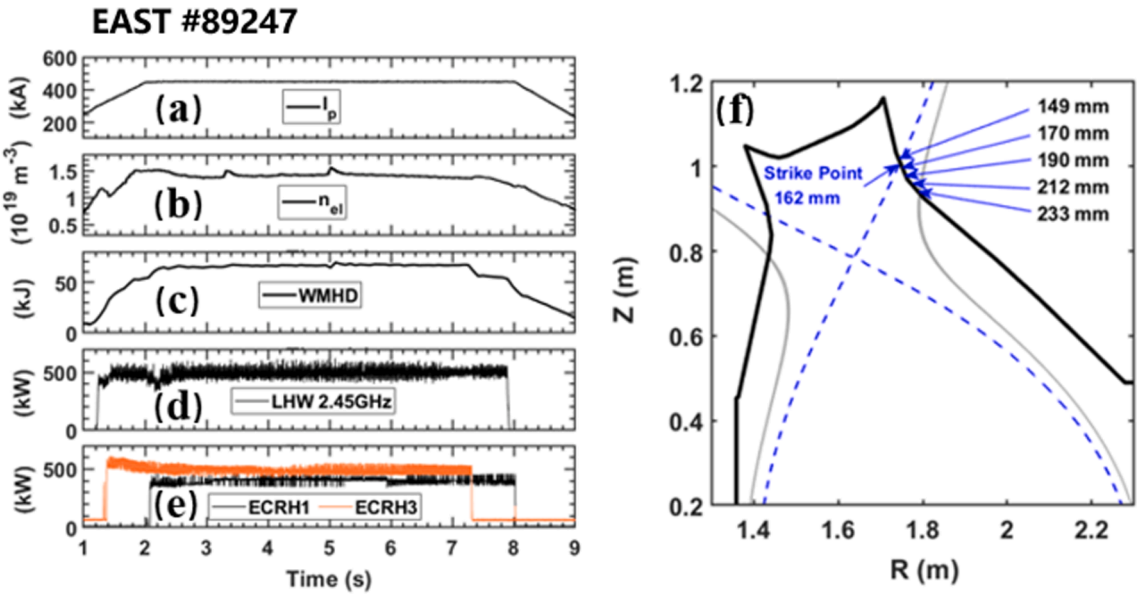

Fig. 7. Time evolutions of (a) the plasma current, (b) the line-averaged electron density, (c) the stored energy, (d) 0.5 MW 2.45 GHz LHW and (e) 0.9 MW ECRH, (f) the magnetic configuration at 4.5 s for #89247.

change of sputtering efficiency of W atoms and WD molecules, respectively.

In a typical upper single null (USN) divertor discharge #95991, T_{et} at the peak positions of WD and WI radiance keeps almost the same from 7.2 s to 7.5 s as shown in Fig. 10(a). Thus the time range from 7.2 s to 7.5 s in #95991 is used to compare the variation of the sputtering efficiency of WD molecules and W atoms.

Discharge #95991 is sustained by 2 MW LHW, 0.9 MW ECRH and 2 MW NBI heating power at a line-averaged density of $_{el} = 3 \times 10^{19}$ m^{-3}. The distribution of the ion flux density (UO j_s), as well as WI and WD radiance along the W target in this discharge are shown in Fig. 9. It can be seen that the WI radiance is mostly concentrated near the strike point, consistent with the distribution of the UO j_s. While the peak WD radiance is farther away from the strike point, where the UO j_s is obviously weaker.

Fig. 10 compares the temporal evolution of main parameters from 7.2–7.5 s at 159 mm and 191 mm. Fig. 10(a) shows that during 7.2–7.5 s, the T_{et} at these two positions is equal, which means the same impact energy E_{in}. The same Ph_{WI}/Γ_{ion} at 159 mm and 191 mm in Fig. 10(b) indicates the same sputtering efficiency of W atoms at the two positions, demonstrating a pure physical sputtering characteristic, i.e. the dependence on T_e. By contrast, Fig. 10(c) shows that the higher sputtering efficiency of WD molecules appears at 191 mm despite the same T_{et} at the two positions. There should be some element other than impact energy influencing the WD sputtering efficiency. Fig. 10(d) compares the heat flux at the two positions [27,28]. The heat flux at 191 mm is around 0.5 MW/m^2, lower than 0.6 MW/m^2 at 159 mm. Normally, the higher heat flux would lead to higher target temperature which could influence the D content in the thin surface layer [29].

The influences of heat flux on the sputtering efficiency of WD molecules and W atoms were also compared for the temporal evolution. The H-mode discharge #98765 is with a lower single null (LSN) configuration and sustained by 2.5 MW LHW and 1.45 MW ECRH. The plasma current I_p at the top phase is 500 kA and lasts 20 s. The line-averaged electron density $_{el}$ slowly rises from 1.6×10^{19} m^{-3} to 2.5×10^{19} m^{-3} as shown in Fig. 11(a). Fig. 11(b) and (c) show an increasing particle flux density (LO j_s) and decreasing electron temperature (LO T_e) at the lower outer divertor with the increasing electron density $_{el}$. During 9–15 s, the heat flux hitting the divertor drops from 1.3 MW m^{-2} to 0.3 MW m^{-2} (Fig. 11(d)).

To minimize the influence of T_e on the photon emission efficiency, two periods in the discharge with relative constant T_e are selected for analysis as shown in Fig. 12. Both WD molecule and W atom sputtering present a similar rising trend with the heat flux when the heat flux is low (0.3 MW/m^2–0.6 MW/m^2 in Fig. 12(a)). When the heat flux rises above 0.6 MW/m^2, a downward trend of WD sputtering efficiency can be observed with increasing heat flux while W atom sputtering efficiency still keeps a rising trend with the heat flux, suggesting a different

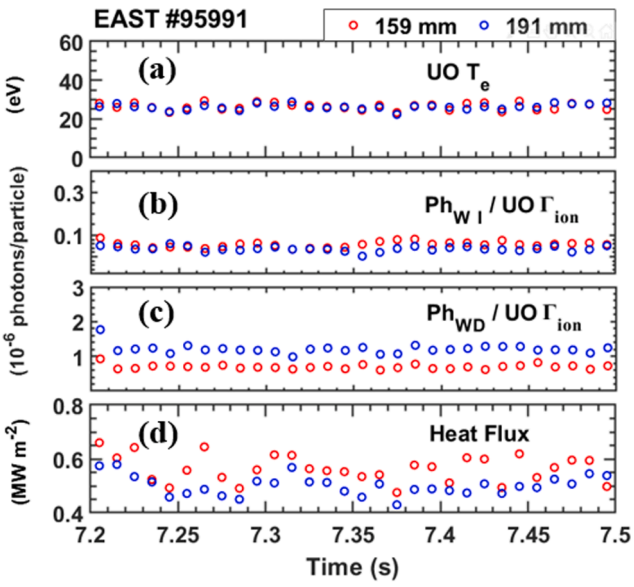

Fig. 10. Time evolutions of (a) the electron temperature (T_{et}), (b) the ratio Ph_{WI}/Γ_{ion}, (c) the ratio Ph_{WD}/Γ_{ion} of the two positions (159 mm and 191 mm away from the UO divertor corner). And time evolutions of (d) the heat flux of the two positions.

sputtering mechanism for WD molecule sputtering compared with W atom sputtering.

Fig. 12(a) shows the evolution of Ph_{WI}/Γ_{ion} and Ph_{WD}/Γ_{ion} as functions of heat flux during 13–14 s when the value of heat flux is relatively low and LO T_e changes in the range of 14–23 eV. Assume that the *S/XB*-values for WI and the *D/XB*-values for WD are respectively comparable in the range of LO $T_e = 14$ eV and LO $T_e = 23$ eV [4,16]. So that the ratio Ph_{WI}/Γ_{ion} and Ph_{WD}/Γ_{ion} can represent the sputtering efficiency of W atoms and WD molecules in this period. As the heat flux increases, the sputtering efficiency of W atoms keeps increasing while the sputtering efficiency of WD molecules increases first and then decreases after reaching a peak.

Fig. 12(b) shows the evolution of Ph_{WI}/Γ_{ion} and Ph_{WD}/Γ_{ion} as functions of heat flux during 10–11 s when the value of heat flux is relatively high and LO T_e changes in the range of 40–45 eV. In this phase, as the heat flux increases, the sputtering efficiency of W atoms remains at a high level, while the sputtering efficiency of WD molecules significantly reduces. The results may be the influence of the chemical sputtering character of WD sputtering – the WD sputtering has a significant dependence on the deuterium content in the W surface layer [4]. The increasing surface temperature of the W target caused by the increasing

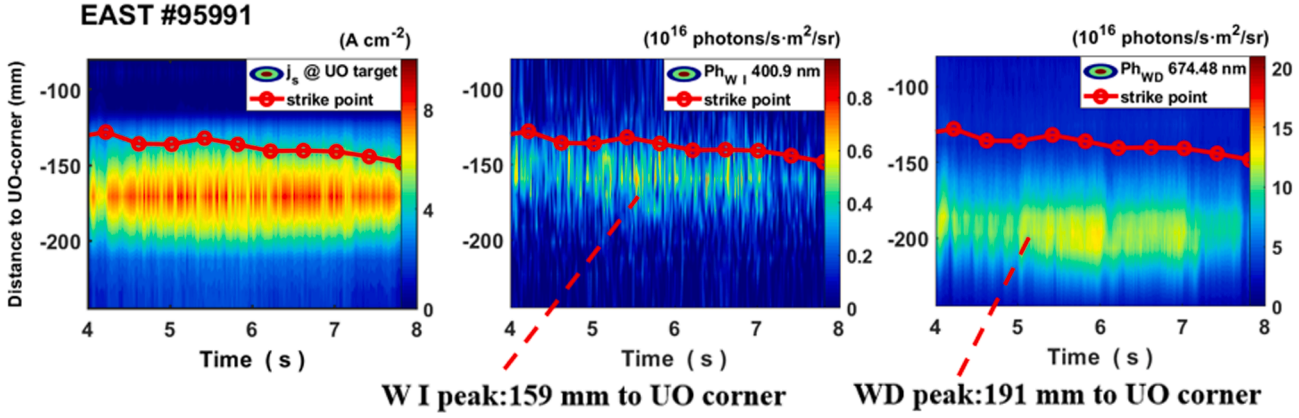

Fig. 9. The distribution of the ion fluxes (UO j_s), as well as WI and WD radiance along the W target of discharge #95991.

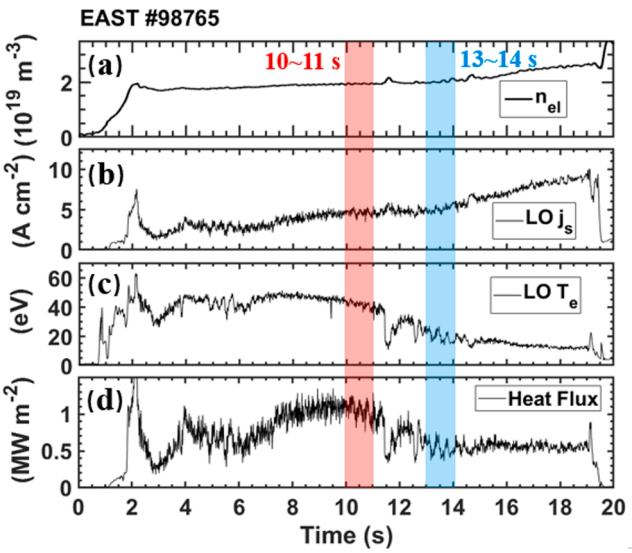

Fig. 11. Time evolutions of (a) the line-averaged electron density $_{el}$ in the core plasma, (b) the particle flux density (j_s), (c) the electron temperature (T_e) and (d) the heat flux in the lower outer (LO) divertor of discharge #98765.

heat flux can lead to more desorption of the deuterium in the surface layer [30,31], which may be the possible reason for the decrease in the sputtering efficiency of WD molecules. While for W atoms, since it is purely physical sputtering, its sputtering efficiency is mainly affected by the impact energy. Therefore, in Fig. 12(a) its sputtering efficiency continues to rise due to the rise of LO T_e, and in Fig. 12(b) its sputtering efficiency remains at a high level since LO T_e remains at a high level (The relationship between LO T_e and heat flux of discharge #98765 in LO divertor is shown in Fig. 13).

It is observed in EAST that the decrease of the sputtering efficiency of WD with the increase of the heat flux hitting the W target is often accompanied by the rise of the line intensity of D_δ (410 nm) normalized to the particle flux (Γ_{ion}) at the divertor, which may imply the enhanced D desorption at the W surface.

Fig. 14 shows the evolutions of the ion flux (j_s), the electron temperature (T_e), the WD radiance, the D_δ (410.06 nm) radiance, and the heat flux around the strike point in the upper outer (UO) divertor in discharge #87707 from 2.6 s to 3.2 s. In this phase the ion flux density UO j_s keeps increasing with time while the electron temperature UO T_e remains almost unchanged, therefore the heat flux increases with time.

During the phase with constant UO T_e, the ratio Ph_{WD}/Γ_{ion} and $Ph_{D\delta}/\Gamma_{ion}$ can qualitatively reflect the sputtering efficiency of WD molecules and the deuterium desorption rate at the divertor target. A higher ratio of $Ph_{D\delta}/\Gamma_{ion}$ may mean increased deuterium evaporation/dissociation from the W surface layers, thus a lower deuterium retention ratio in the W target [30,31].

Fig. 15 plots the ratio Ph_{WD}/Γ_{ion} against $Ph_{D\delta}/\Gamma_{ion}$ from 2.6 s to 3.2 s in #87707 when the T_{et} keeps nearly constant. It can be seen that Ph_{WD}/Γ_{ion} presents a decreasing trend with $Ph_{D\delta}/\Gamma_{ion}$, indicating that the sputtering efficiency of WD molecules decreases with the reduction of deuterium retention in the W target. The increasing $Ph_{D\delta}/\Gamma_{ion}$ should result from the increasing heat flux. The increase of heat flux could elevate the surface temperature and benefit the deuterium release from the W surface, which may influence the formation of WD molecules at the W surface layer. Therefore, the changes in deuterium content in the W surface layers may be responsible for the dependence of WD sputtering on the heat flux hitting the W divertor, which is consistent with research result of Brezinsek et al. [4]. The near-surface fuel content in W may affect the WD sputtering efficiency - the chemical sputtering character of CAPS. Different D content in the W surface at different target temperatures could play an important role here.

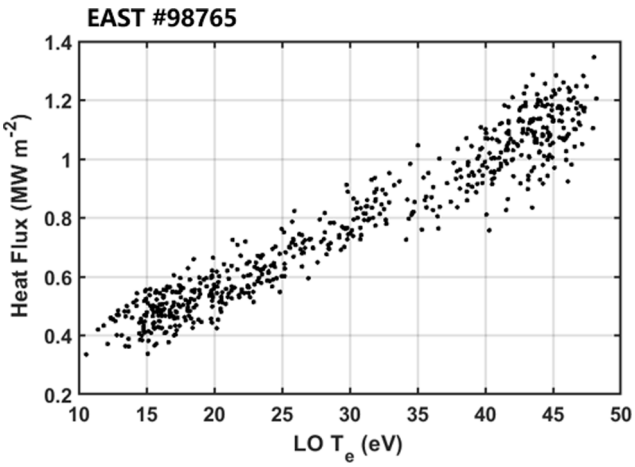

Fig. 13. The relationship between LO T_e and heat flux of discharge #98765 in LO divertor.

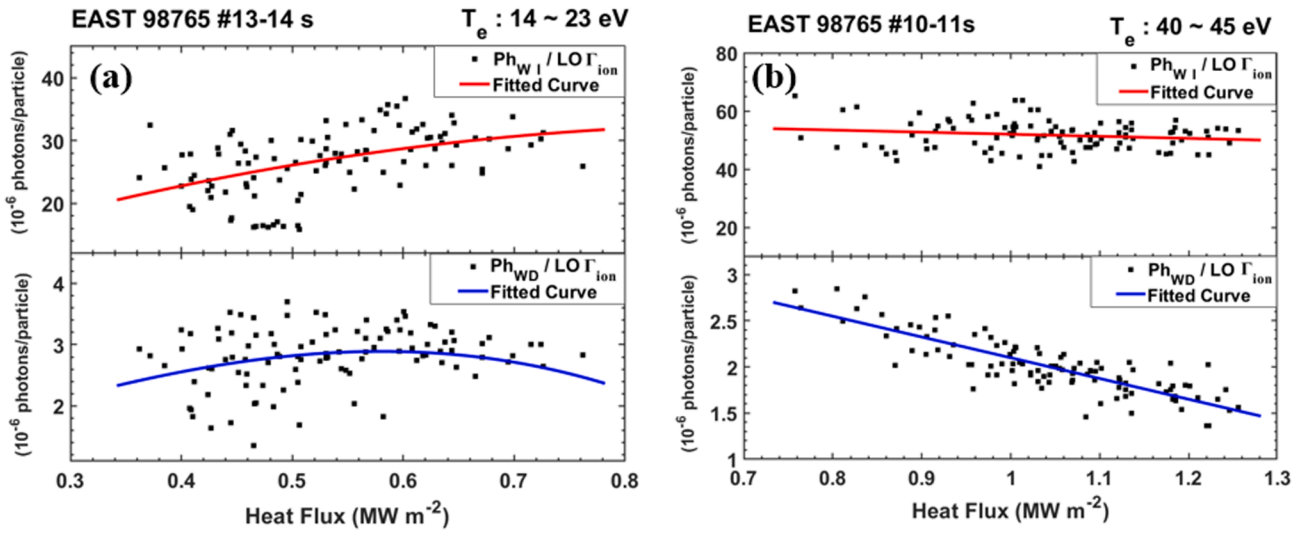

Fig. 12. The evolutions of Ph_{WI}/Γ_{ion} and Ph_{WD}/Γ_{ion} as a function of heat flux hitting the LO divertor (a) during 13 s to 14 s and (b) during 10 s to 11 s.

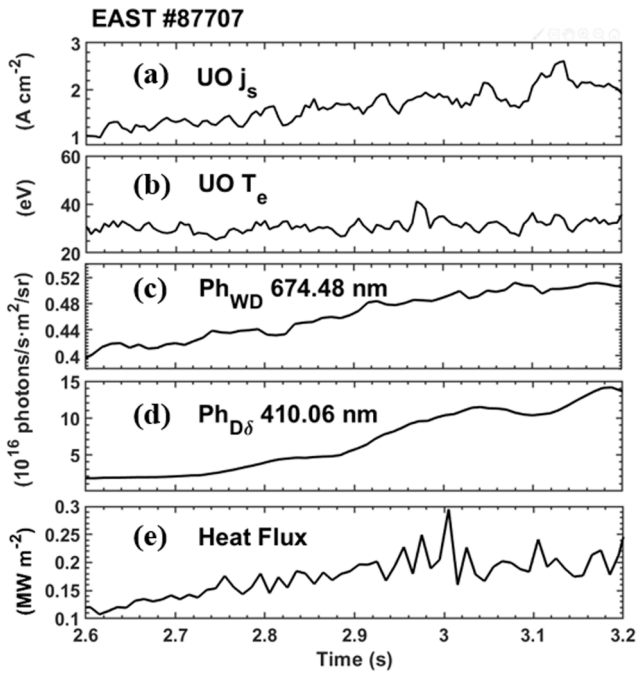

Fig. 14. Time evolutions of (a) the ion flux (j_s), (b) the electron temperature (T_e), (c) the WD radiance, (d) the Dδ radiance, and (e) the heat flux in the upper outer (UO) divertor of discharge #87707.

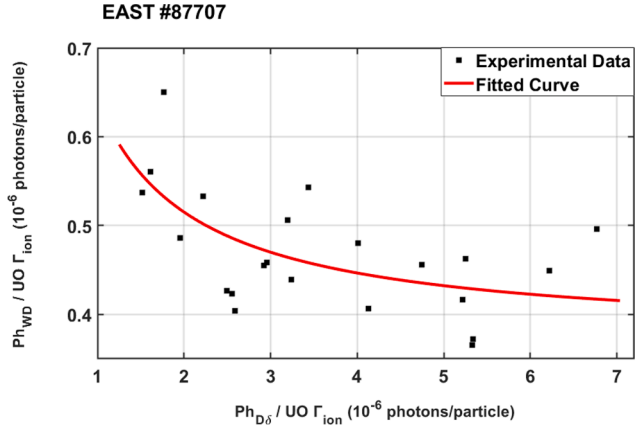

Fig. 15. The relationship between the ratio of Ph_{WD}/Γ_{ion} and $Ph_{D\delta}/\Gamma_{ion}$ during 2.6–3.2 s.

4. Summary and conclusion

WD molecule sputtering is observed via spectroscopic measurement in the EAST W divertor and compared with W atom sputtering by defining Ph_{WD}/Γ_{ion} and Ph_{WI}/Γ_{ion} as the sputtering efficiencies of WD molecules and W atoms, respectively. The dependences of Ph_{WD}/Γ_{ion} on target T_{et} is obtained and an energy threshold at $T_{et} = 8$ eV is found for WD molecule sputtering in the observed discharge. The experimental comparison shows that the sputtering of W atoms is mostly concentrated near the strike point, while the sputtering distribution of WD molecules is relatively wide, extending to the far SOL region where impact energy of incident ions is lower than that around the strike point. These indicate that the sputtering energy threshold of WD molecules in EAST is smaller than that of W atoms.

The other important difference between WD molecule sputtering and W atom sputtering is the dependence on heat flux hitting the W target. When the heat flux increases, the sputtering efficiency of WD molecules first increases and then decreases, while the sputtering efficiency of W atoms continues to increase with the heat flux. Similar dependences of the sputtering efficiency of WD molecules and W atoms are also found on target T_{et}, due to the proportional relationship between heat flux and T_{et}. These observations indicate that in addition to the impact energy (T_{et}), there is another element influencing WD sputtering efficiency, which is different from W atom sputtering efficiency, a typical physical sputtering with a mere dependence on the impact energy (T_{et}). Further study shows that the WD sputtering efficiency has a decreasing trend with the increasing deuterium desorption rate. This could imply that the near-surface fuel content in W may be another important factor influencing the WD sputtering efficiency. The decreasing WD molecule sputtering efficiency with increasing heat flux is most likely due to the reduced deuterium content in the W surface layer caused by the increased heat flux, thus the elevated target temperature. So the WD molecule sputtering could be ascribed to chemically assisted physical sputtering.

CRediT authorship contribution statement

Q. Zhang: Conceptualization, Methodology, Validation, Formal analysis, Investigation, Writing – original draft, Writing – review & editing. **F. Ding:** Conceptualization, Methodology, Validation, Formal analysis, Investigation, Supervision, Project administration, Funding acquisition. **S. Brezinsek:** Conceptualization, Methodology, Validation. **L. Yu:** Resources, Validation. **L.Y. Meng:** Resources, Validation. **P.A. Zhao:** Writing – review & editing, Validation, Visualization. **D.W. Ye:** Writing – review & editing, Data curation. **Z.H. Hu:** Writing – review & editing, Validation. **Y. Zhang:** Resources, Validation. **R. Ding:** Writing – review & editing, Validation. **L. Wang:** Resources, Writing – review & editing, Validation. **G.-N. Luo:** Project administration.

Declaration of Competing Interest

The authors declare that they have no known competing financial interests or personal relationships that could have appeared to influence the work reported in this paper.

Data availability

Data will be made available on request.

Acknowledgments

This work was supported by the National Key Research and Development Program of China (Grant Nos. 2017YFE0301300 and 2018YFE0303103), the National Natural Science Foundation of China (Grant Nos. 12192283 and 12022511), the JSPS-CAS Bilateral Joint Research Project (Grant No. GJHZ201984), the Key Research Program of Frontier Sciences of CAS (Grant No. ZDBS-LY- SLH010), and the Major Science and Technology Infrastructure Maintenance and Reconstruction Projects of Chinese Academy of Sciences (2021).

References

[1] S.P.T. Hirai, et al., Nucl. Mater. Energy 9 (2016) 616–622.
[2] R. Neu, et al., Phys. Scr. T138 (2009) 014038.
[3] R. Neu, et al., Phys. Plasmas 20 (2013) 056111.
[4] S. Brezinsek, et al., Nucl. Mater. Energy 18 (2019) 50–55.
[5] A. Kirschner, et al., Nucl. Mater. Energy 18 (2019) 239–244.
[6] T. Pütterich, et al., Nucl. Fusion 50 (2010) 025012.
[7] I. Murakami, et al., Nucl. Mater. Energy 26 (2021) 100923.
[8] L. Cao, et al., J. Fusion Energ. 34 (2015) 1451–1456.
[9] G.S. Xu, et al., Nucl. Fusion 61 (2021) 126070.
[10] X.H. Chen, et al., Nucl. Fusion 61 (2021) 046046.
[11] M. Mayer, et al., J. Nucl. Mater. 363–365 (2007) 101–106.
[12] L. Ballauf, et al., Int. J. Mass Spectrom. 448 (2020) 116252.
[13] H.M. Mao, et al., Rev. Sci. Instrum. 88 (2017) 043502.
[14] H.M. Mao, et al., Nucl. Mater. Energy 12 (2017) 447–452.
[15] J.C. Xu, et al., Rev. Sci. Instrum. 87 (2016) 083504.

[16] R. Neu, et al., AIP Conf. Proc. 901 (2007) 85.
[17] T. Abrams, et al., Phys. Plasmas 26 (2019) 062504.
[18] H. Kawazome, et al., Plasma Fusion Res. 5 (2010) S2073.
[19] T. Nakano, et al., Nucl. Fusion 42 (2002) 689–696.
[20] P.C. Stangeby, Plasma Bound. Magn. Fus. Dev. (2000).
[21] S. Liu, et al., J. Appl. Phys. 108 (2010) 073302.
[22] E. Salonen, et al., Phys. Rev. B 63 (2001) 195415.
[23] B. Yang, et al., Chin. J. Atom. Mole. Phys. 19 (2002) 42–44.
[24] A. Pospieszczyk, et al., J. Phys. B: At. Mol. Opt. Phys. 43 (2010) 144017.
[25] G.-N. Luo, et al., Nucl. Fusion 57 (2017) 065001.
[26] D. Nishijima, et al., Plasma Phys. Controll. Fusion 50 (2008) 125007.
[27] L.Y. Meng, et al., Plasma Phys. Controll. Fusion 62 (2020) 065008.
[28] L. Wang, et al., Nucl. Fusion 59 (2019) 086036.
[29] C. Sang, et al., Nucl. Fusion 52 (2012) 043003.
[30] C. Sang et al., EPS2011 38th Conference on Plasma Physics, 2011, P5.058.
[31] J. Roth, et al., Phys. Scr. 145 (2011) 014031.